Organogenesis, 11:58–74, 2015
Published with license by Taylor & Francis Group, LLC
ISSN: 1547-6278 print / 1555-8592 online
DOI: 10.1080/15476278.2015.1072661

Creation and implantation of acellular rat renal ECM-based scaffolds

Andrea Peloso,[1,*,#] Jacopo Ferrario,[1,#] Benedetta Maiga,[1] Ilaria Benzoni,[1] Carolina Bianco,[1] Antonio Citro,[2] Manuela Currao,[3] Alessandro Malara,[3] Annalisa Gaspari,[5] Alessandra Balduini,[3,4] Massimo Abelli,[1] Lorenzo Piemonti,[2] Paolo Dionigi,[1] Giuseppe Orlando,[6,##] and Marcello Maestri[1,##]

[1]Dept. of General Surgery; IRCCS Policlinico San Matteo; Dept. of General Surgery; University of Pavia, Pavia, Italy
[2]Beta Cell Biology Unit; Diabetes Research Institute; San Raffaele Scientific Institute, Milan, Italy
[3]Dept. of Molecular Medicine, Biotechnology Laboratories, IRCCS Policlinico San Matteo; University of Pavia, Pavia, Italy
[4]Dept. of Biomedical Engineer; Tufts University; Medford, MA USA
[5]University of Pavia; Animal Facility Center Botta 2, Pavia, Italy
[6]Wake Forest School of Medicine; Winston Salem, NC USA

[#]Andrea Peloso and Jacopo Ferrario share the first Authorship.

[##]Giuseppe Orlando and Marcello Maestri share the last authorship.

ABSTRACT. Kidney transplantation is the only potentially curative treatment for patient facing end-stage renal disease, and it is now routinely used. Its use is mainly limited by the supply of transplantable donor organs, which far exceeds the demand. Regenerative medicine and tissue engineering offer promising means for overcoming this shortage. In the present study, we developed and validated a protocol for producing acellular rat renal scaffolds.

Left kidneys were removed from 26 male Lewis rats (weights: 250–350 g) and decellularized by means of aortic anterograde perfusion with ionic and anionic detergents (Triton X-100 1% and SDS 1%, respectively). 19 scaffolds thus obtained (and contralateral native kidneys as controls) were deeply characterized in order to evaluate the decellularization quality, the preservation of

*Correspondence to: Andrea Peloso; Email: andreapeloso@hotmail.it

Received August 28, 2014; Revised April 3, 2015; Accepted July 9, 2015.

extracellular matrix components and resultant micro-angioarchitecture structure. The other 7 were transplanted into 7 recipient rats that had undergone unilateral nephrectomy. Recipients were sacrificed on post-transplantation day 7 and the scaffolds subjected to histologic studies.

The dual-detergent protocol showed, with only 5 h of perfusion per organ, to obtain thoroughly decellularized renal scaffolds consisting almost exclusively of extracellular matrix. Finally the macro- and the microarchitecture of the renal parenchyma were well preserved, and the grafts were implanted with ease. Seven days after transplant, the scaffolds were morphologically intact although all vascular structures were obstructed with thrombi. Production and implantation of acellular rat renal scaffolds is a suitable platform for further studies on regenerative medicine and tissue engineering.

KEYWORDS. bioscaffold, extracellular matrix, kidney transplantation, organ bioengineering, rat model, regenerative medicine, scaffold

ABBREVIATIONS. DCD, Donation after cardiac death; ECD, Expanded donor criteria; ECM, Extracellular matrix; ESRD, End-stagerenal disease.

INTRODUCTION

Organ transplantation is acknowledged as one of modern medicine's most important achievements. According to the United Network for Organ Sharing [UNOS], the number of patients on transplant waiting lists in the United States as of 11 February 2015 was 123,206 (www.unos.org). This figure highlights the main hurdle to the wider use of this solution: the demand for transplantable organs continues to grow, whereas the number of available organs seems to have plateaued in recent years. The result is a dramatically widening gap between supply and demand.

Renal transplantation is currently the most effective treatment for end-stage renal disease (ESRD) that represents one of the primary mortality reason globally. In recent years, noteworthy progress has been made in our understanding of the mechanisms of rejection[1,2] and the factors that can reduce the function of the transplanted kidney.[3] In addition, new immunosuppressant regimes have been developed which have reduced the morbidity and mortality associated with renal transplant.[4] These advances have increased the number of patients who are eligible for renal transplantation although the availability of donor organs has remained stable.[5]

Various strategies have been developed to increase the number of available renal grafts, including the elaboration and adoption of Expanded Donor Criteria (ECD) [6,7] and the practice of donation after cardiac death (DCD).[8,9] Their use has lowered mortality rates among patients on waiting lists, but the chances of actually receiving a kidney remain slim: only 9.65% undergo transplantation after a wait of 12 months, and the success rate after 36 months is only 21.65% (www.unos.org). In light of these figures, any different approach that is potentially capable of expanding the donor pool has to be considered.

Regenerative medicine is an innovative multidisciplinary field that is attracting growing interest combining natural materials bioengineering, cellular seeding and organ transplantation. Its main goal is to restore the physiological properties that cells, tissues, and organs lose as a result of a disease.[10] In recent years, it has been used in tandem with bioengineering in an attempt to solve the problem of donor organ shortage. The final aim is to develop effective alternative solutions based on tissue engineering, more specifically, on the repopulation of natural or synthetic "scaffolds" with the patient's own cells, a process that exploits the macro-and microstructural properties of the scaffold itself.[11,12] This approach has

already been successfully used to create simple, hollow anatomic structures, such as blood vessels,[13] upper airway segments,[14] and lower segments of the urogenital system,[15] but the real challenge is to reconstruct functional, complex, parenchymal organs, such as kidney, liver, pancreas, or lung.[16] Here too possibilities for creating 3-dimensional scaffolds suitable for subsequent cell growth have been explored.[17,18] Numerous studies have shown that organic, acellular heart and liver scaffolds composed entirely of extracellular matrix (ECM) can indeed be created,[19-21] but relatively little is known about the effective morphometric preservation of the organ-specific matrix architecture after the decellularization and on the post-transplant behavior of these structures.

In the present study we analyzed preliminary data on an experimental model of production and transplant of ECM-based scaffolds from rat kidneys. Our aims were (i) to create and simplify a protocol for producing ECM-based rat renal scaffolds, (ii) to evaluate the resulting scaffolds in terms of the preservation of the structural (biochemical and morphological) integrity, (iii) to assess the macrostructural integrity of the scaffold under conditions of physiological organic pressure following orthotopic transplantation, (iv) to evaluate the post-transplant tolerability of the scaffold.

RESULTS

Creation of decellularized renal scaffolds

We developed a dual-detergent protocol that reduces time of perfusion (5 h per organ) while delivering high-quality decellularization status. Infusion of the detergent solutions was accompanied by macroscopic transformations in the appearance of the kidney, which lost its native color as the blood and cellular components were removed and ultimately assumed an almost-transparent appearance (**Fig. 1** Panel 1 and 2). At the end of the decellularization process, each of the scaffolds we prepared maintained complete renovascular networks, from the hilum to the outermost areas of the periphery (**Fig. 6B**).

Histological and fluorescent microscopic studies of the scaffolds

H&E staining of non-implanted renal scaffolds revealed complete preservation of the renal parenchymal architecture, with intact blood vessels and glomeruli, and the absence of cellular material. The prevalence of eosinophilic structures indicated that the tissue was composed largely of collagen. Masson's Trichrome and Picrosirius red staining confirmed the presence of intact 3-dimensional ECM structures composed predominantly of collagen, and Alcian Blue staining detected the presence of proteoglycans in the matrix staining. DAPI positivity, which was observed in all the native kidney tissue controls, was absent in all the scaffolds, confirming the absence of residual DNA (**Figs. 1, 2**). These data was also indirectly confirmed by DNA quantification. Immunofluorescent microscopy showed full expression in the scaffolds of the major ECM proteins (types I, III, and IV collagens, fibronectin, laminin), with cortical and medullary expression patterns that were not significantly different from those of respective contralateral controls. The decellularization protocol thus appeared to successfully eliminate the cellular component without altering the ECM protein composition (**Figs. 2, 3**).

DNA quantification

DNA, considered as the real xenogeneic insult for the host response,[23] was quantified as an indirect marker of decellularization status. Renal scaffold showed a statistical significant reduction of the DNA content compared to the native one (Native: AVG 94.6 ng/μl mean $\pm$1.67; Decellularized: AVG 7.23 ng/μl mean $\pm$1.95) (% DNA content removal: -92.35; $p = 0.028$) (**Fig. 4**).

Laminin and Collagens quantification

Laminin evaluation showed a statistically significative reduction respectively from native

FIGURE 1. Decellularization process and extracellular matrix analysis of rat native kidney compared with rat kidney scaffold. Panel 1 Representative images of donor kidney immediately after the harvesting (**A**), after perfusion with 1% Triton X-100 solution (**B**), and after final wash with 1% SDS detergent (**C**). H&E stainings (10X magnification) for each picture confirm the progressive cellular removal with the simultaneous preservation of 3D structure composed entirely by ECM (scale bar: 200 μm) Panel 2 H&E stainings (first row) show the complete loss of all cellular components from renal native parenchyma. Scaffolds' tissue positivity for Masson's' Trichrome (second row), Picrosirius Red (third row) and Alcian Blue staining (forth row) confirm the preservation of glycosaminoglycan (GAGs), collagen fibrils and mucins in the decellularized renal extracellular matrix, even with qualitative difference. All the stainings show the preservation of typical organ-specific and region-specific geometry of both renal inner and outer regions (medulla and cortex). Magnification 10x; scale bar: 200 μm (for each image).

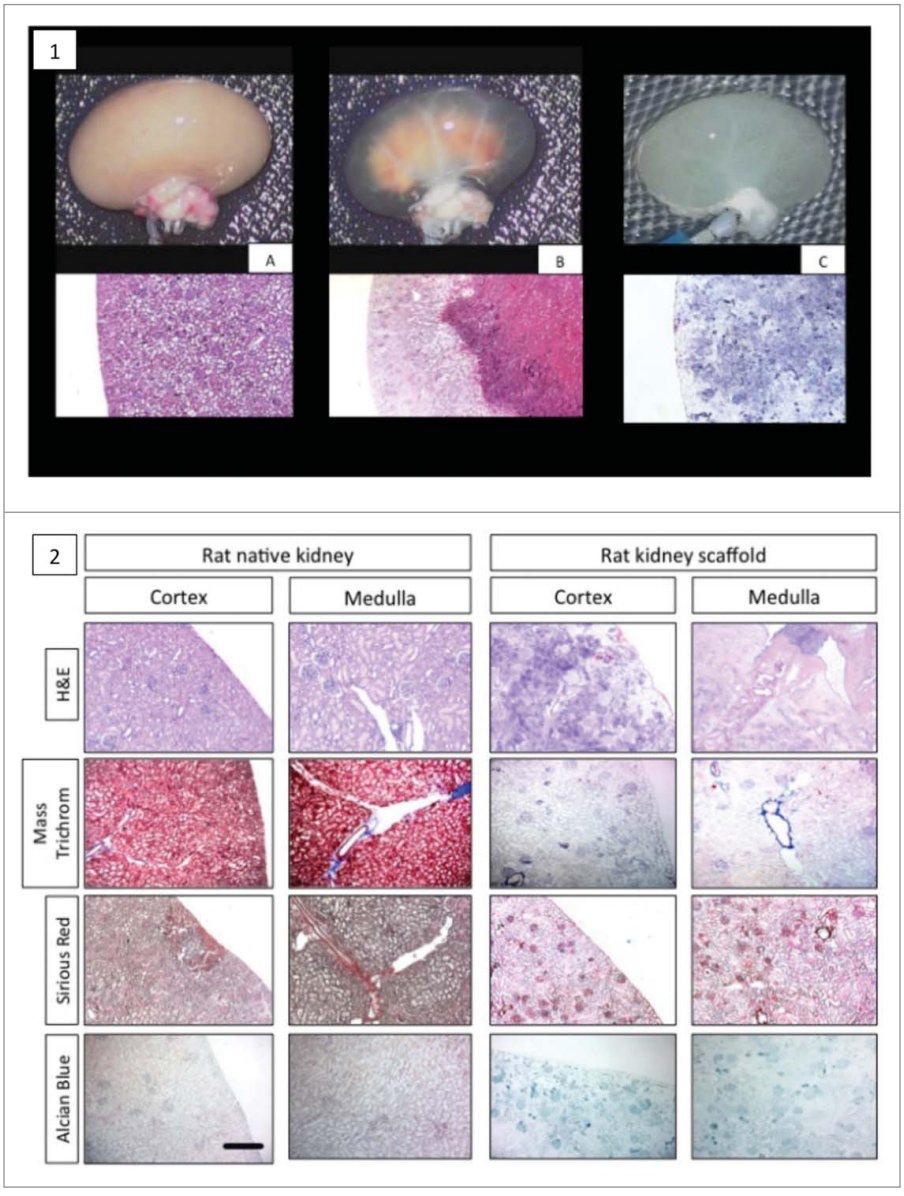

FIGURE 2. Representative immunofluorescence analysis of ECM in normal and decellularized rat kidneys. Images show the distribution of type I, type III, type IV collagens, laminin and fibronectin (green) in rat kidney sections (cortex and medullar portions) before and after decellularization. Magnification 20x; scale bar 100 μm (for each).

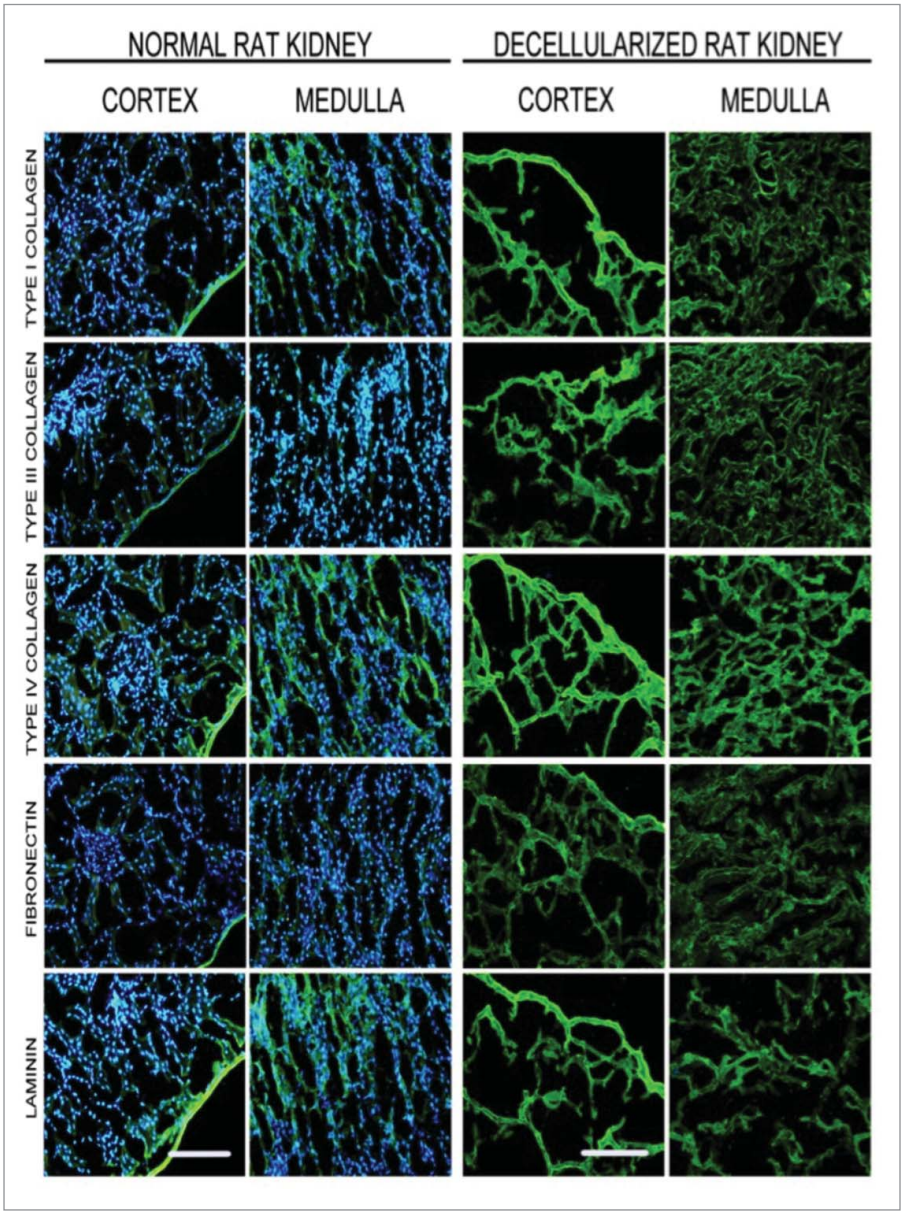

and TNX-perfused groups, and native and acellular scaffolds (Native 827,019 $\pm$ 12.34 $p <$ 0.001 and TNX-perfused 631,531 $\pm$ 16.08 p $=$ 0.0028). Otherwise, no significative difference was observed between TNX and acellular groups (**Fig. 3, 4**).

Quantitative collagens analysis demonstrated no significative statistical difference in kidney before and after the decellularization (Native AVG 141,885 mean $\pm$13,454 μg/mg dry-tissue; Scaffold AVG 167,997 mean $\pm$21,749. N $=$ 3 for each group) (**Fig. 4**).

FIGURE 3. Laminin evaluation and comparison between native, TNX-100-flushed and acellular renal scaffold Images show laminin preservation during the decellularization process. First row illustrates laminin assay (upper left), DAPI staining (upper central) and merged picture (upper right) on native kidney Second row shows laminin assay (middle left), DAPI staining (middle central) and merged picture (middle right) performed on renal organ perfused with TNX only. Third row displays laminin assay (lower left), DAPI staining (lower central) and merged pictured executed on final acellular kidney scaffold. At the end of the process laminin was well conserved whereas, interestingly, DAPI staining during the process looks gradually decreasing. This qualitative data suggest that our protocol is soft enough to preserve laminin but, at the same time, can progressively remove DNA material.

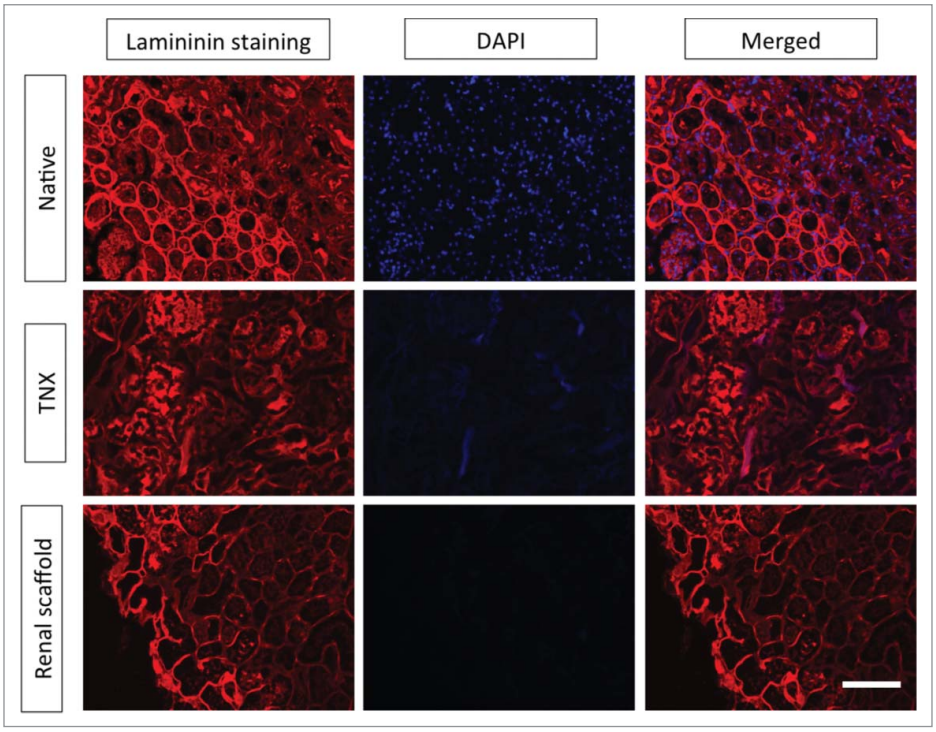

Morphometrical analysis of corrosion-casted glomerular samples

Proposed vascular corrosion cast protocol effectively manufactured rat whole-kidney cast from both groups of study (native = 3 and acellular scaffold = 3) preserving the entire angioarchitecture down to the capillary level. SEM analysis revealed morphological maintenance of afferent and efferent glomerular arterioles and of the typical glomerular angiostructure (**Fig. 5**). Morphometric measurements from both groups were acquired and analyzed. Native glomerular afferent arterioles averaged diameter was 15.43 $\pm$ 0.2783 μm whereas the averaged diameter from scaffold glomerular afferent arterioles was 8,967 $\pm$ 0.2514 μm with a statistically significative reduction of -43% [p-value < 0.0001]. Native efferent arterioles averaged diameter was 12.60 $\pm$ 0.2609 μm and the averaged diameter from scaffold efferent arterioles was 6,867 $\pm$ 0,1333 μm with a statistically significative reduction of -45% [p-value < 0.0001]. Glomerular volumetric calculations showed that averaged native glomerular volume was 1,200e + 006 $\pm$ 17424 μm whereas average glomerular volume from renal scaffolds was 558836 $\pm$ 20099 μm with a statistically reduction of -46% [p-value < 0.0001](**Fig. 5**).

FIGURE 4. DNA quantification, Collagen quantification and Laminin quantification Comparison DNA quantification comparison (upper left graph) between Native and Scaffold group evidently show complete DNA clearance in the scaffold group (−92.35%; p-value = 0.0028; N = 4 for each group). Residual collagen evaluation (upper right graph) shows that collagens are not statistically different between groups (p-value = 0.0649; N = 3 for each group). Laminin quantification was calculated based-on fluorescent intensity demonstrating statistically difference between native and acellular group (p-value = 0.0028; N = 6 for each group) and between native and TNX group (p-value < 0.001; N = 6 for each group). No statistical significance were observed between TNX and scaffold group (p-value > 0.05; N = 6 for each group). All statistical analysis were performed using T-test Mann Whitney.

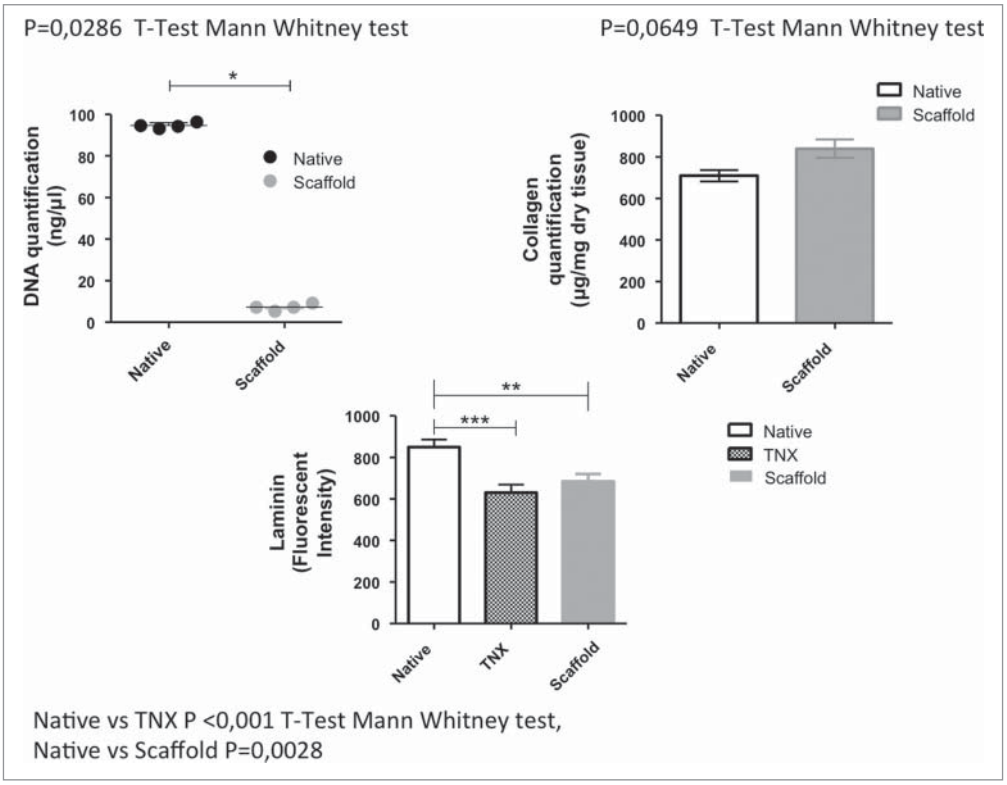

Dynamic recellularization of renal scaffold and cell viability

Acellular kidney scaffold was dynamically seeded with human pancreatic carcinoma cell line (MIA PaCa-2) in a custom made bioreactor that provided optimal conditions for cells viability and vitality (37°C and 21% O2). The seeding process was performed for 24 h under peristaltic perfusion with specific medium. In a short-term culture the cells were homogenously spread inside the parenchyma (from the inner area to the outer). H&E and Ki67 staining confirmed the presence of seeded cells and their proliferative status respectively (**Fig. 6**) and the non-toxicity of the produced matrix.

Scaffold transplantation

Orthotopic transplantation of the renal scaffolds proved to be technically feasible. Although the decellularization process had effectively eliminated the vascular endothelium, the consistency and elasticity of the vascular ECM was sufficient to permit classical arterial anastomosis, which was not

FIGURE 5. Scanning Electron Microscopy SEM images of corrosion casted glomeruli and morphometrical analysis (**A and C**) show representative corrosion casted pictures of native and acellular glomerulus respectively. (**B and D**) illustrate same pictures after virtual highlight of all the measurements taken for morphometric analysis. Glomeruli completely preserved their native original morphology after decellularization process with afferent and efferent arteries and the entire capillary glomerular organization. For afferent artery 3 different measurements were taken (AA1, AA2 and AA3 – red lines). For efferent artery 3 different measurements were acquired (EA1, EA2 and EA3 – blue lines). Glomerular volumetric values were obtained handling each glomerulus as a sphere, measuring 4 different diameters (D1, D2, D3 and D4 – green arrows) that were averaged and then used in the geometrical formula πr^3. Left graph indicates a statistically significative difference between native and acellular group for volumetric value that was reduced in the scaffold (unpaired T-test $p < 0.0001$ N = 30 glomeruli for each group). Statistically significative difference is also observed for afferent and efferent artery between native kidney and acellular scaffold with similar reduction observed for volumes (unpaired T-test $p < 0.0001$ N = 30 arteries –aff and eff-for each group).

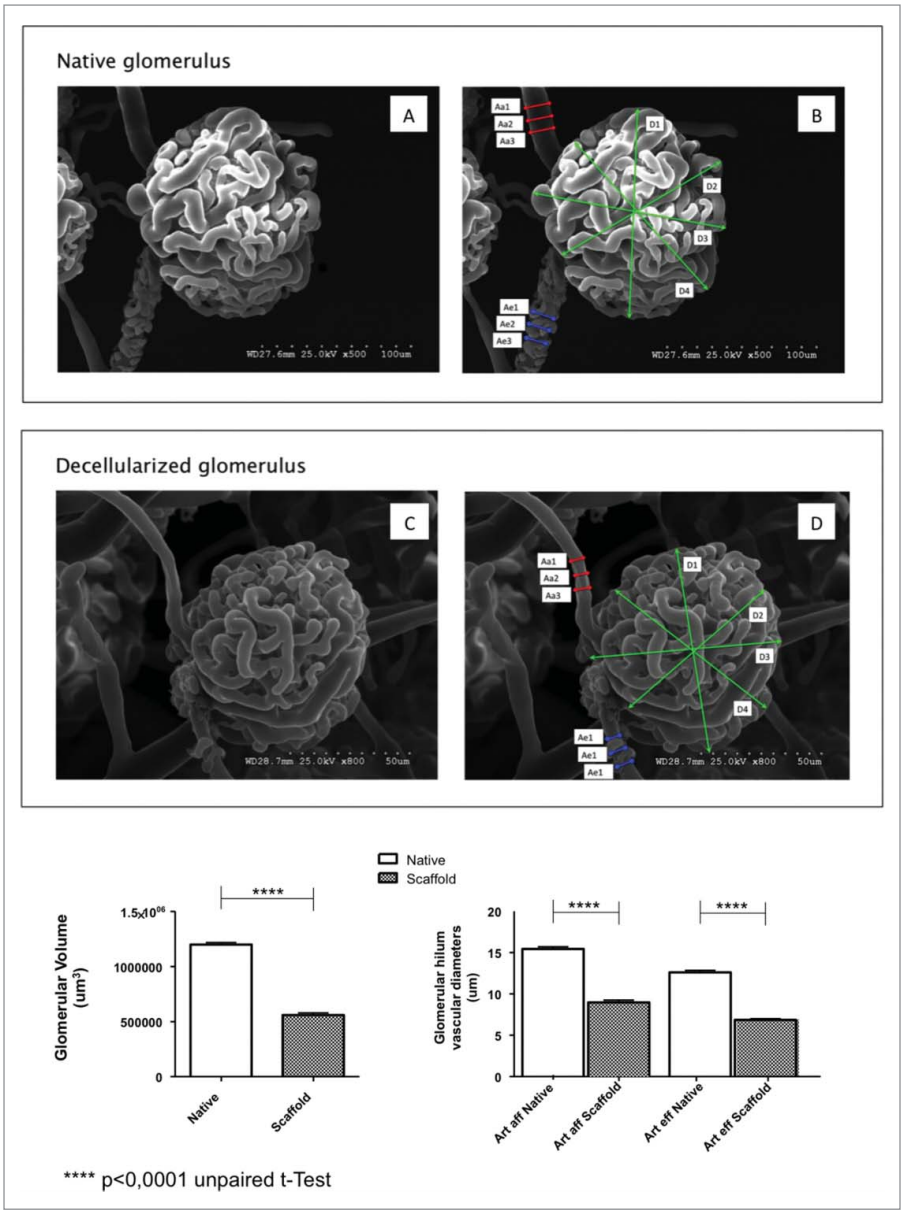

FIGURE 6. Acellular renal scaffold seeding (**A**) Acellular kidney was repopulated in a customized bioreactor providing optimal cells culture conditions (**B and C**) Ki67 staining shows maintenance of proliferation status of cells after 24 h of culturing in a pulsatile system (Magnification: (**A**) 20x; (**B**) 40x).

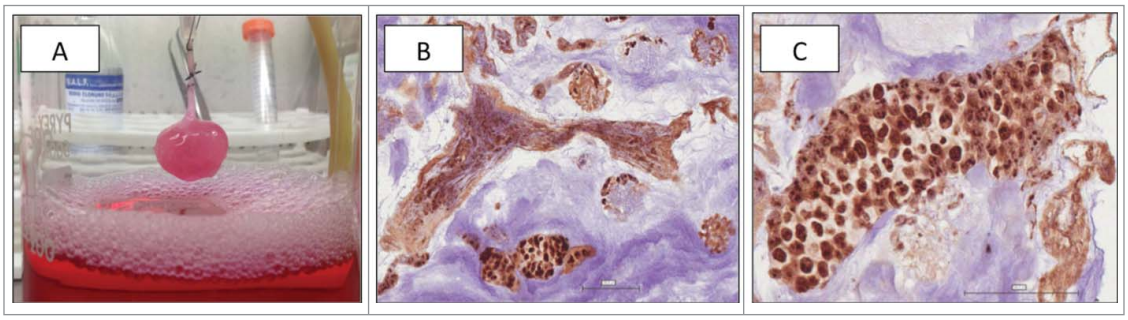

significantly different from the classic aorto-aortic anastomosis used with untreated vessels.

Removal of the vascular microclamps was followed promptly by complete revascularization of the organ. The reperfusion proceeded in accordance with the normal anatomic hierarchy of the kidney, from the hilum to the cortex, with good outflow through the renal vein (**Fig. 7C, D, E and F**). The physiological blood pressure of the recipient animal was well tolerated. In 6/7 implants, no leakage was observed during or after reperfusion. In one exception, the anastomotic site had to be revised to control minor leakage, which was presumably caused mainly by the absence of endothelial cells in the aortic patch used for the arterial anastomoses.

Harvesting and histological examination of renal scaffolds

At the end of the seventh postoperative day, all recipient animals were sacrificed and the scaffolds explanted. In all 7 cases, the graft appeared intact although all of the renal arteries and veins were obstructed with thrombi (**Fig. 8**). The absence of the endothelial layer in these vessels resulted in direct contact between the blood and the collagen of the ECM, which caused massive activation of the coagulation cascade in spite of postoperative antithrombotic prophylaxis. Macroscopic examination of the longitudinally sectioned grafts revealed full preservation of the architecture of the large vessels and the cortical and medullary geometry of the organ.

DISCUSSION

As of now in the United States nearly 1 million patients are affected by ESRD and although organ transplantation is undoubtedly a milestone in the history of medicine, it has recently been referred to as a "halfway technology" capable of alleviating the symptoms of disease without eliminating the underlying causes.[19] It is also important to stress that, as noted above, traditional transplantation is no longer capable of meeting the demand for organs, which has increased dramatically in recent years. These considerations have prompted efforts within the scientific community to identify and develop other solutions to overcome the problem of organ shortage. Promising results have emerged from efforts to combine the forces of regenerative medicine and organ engineering to produce a theoretically inexhaustible supply of organs for transplantation. Important advances have been made even in clinical settings with the successful implantation of regenerated tissues characterized by relatively simple morphological features, including blood vessels, airway or bladder segments, and tubular structures. As for the more structurally complex parenchyma organs, implantation requires the maintenance of a vascular pedicle and preservation of the overall

FIGURE 7. Bench procedure picture: acellular renal graft ready to be implanted and blood reperfusion after renal scaffold implantation (**A**) The renal vein was inserted into the plastic cuff (i) and then extraverted and fixed on it with 7–0 silk suture (ii). (**B**) Vascular network is clearly well preserved even after the elimination of the entire endothelial cells layer. Blue circle shows the cuff positioned on the renal vein and the red circle the aortic patch that will be used for the anastomoses. (**C**) Renal graft just before removal of the vascular clamps. (**D and E**) immediately after clamp removal. (**F**) Enlarged images of the reperfusion phase. During revascularization, the blood follows vessels native hierarchical direction even though the structure is completely lacking in endothelial support. Picture modified from ref. 24.

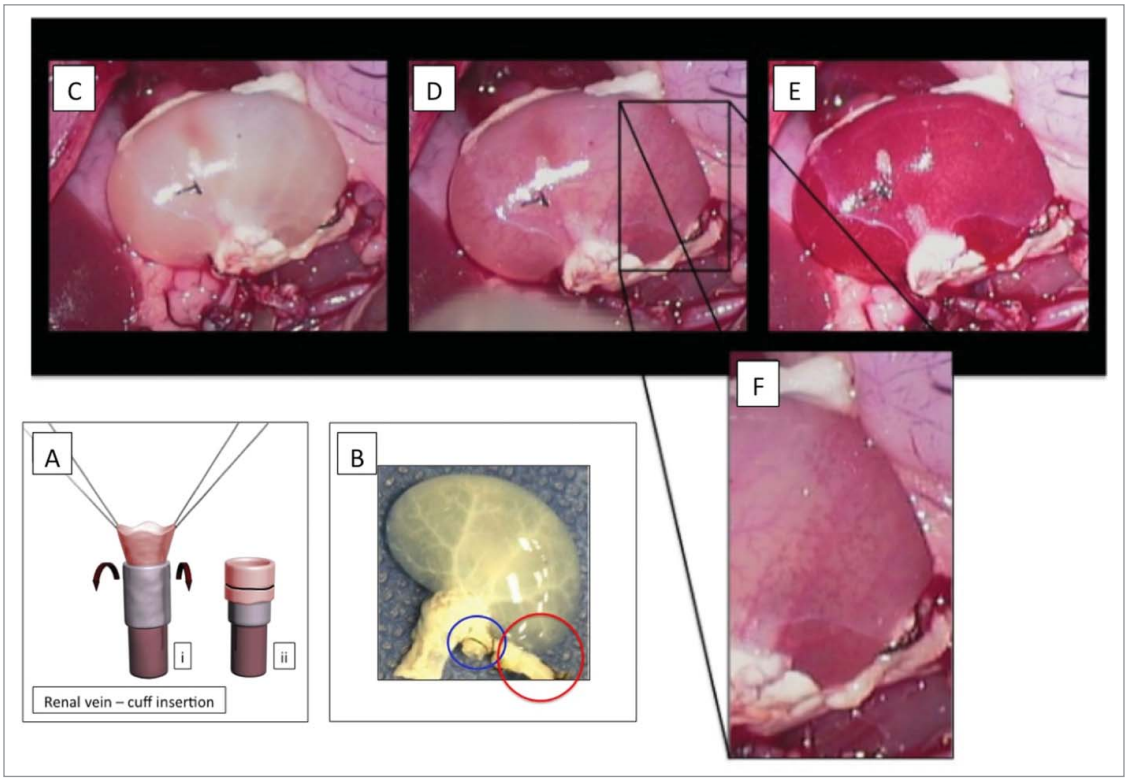

architectural integrity of the organ – both are indispensable for ensuring adequate oxygenation of the transplanted organ.

Decellularization technology focused on whole rat kidney still needs to be complete analyzed and optimized

Recently, in their report, *Caralt et al.* showed a comprehensive investigation about different protocols for rat kidney decellularization.[25] They considered 3 different perfused-based strategies concluding that sequential 26 h Triton/SDS perfusion protocol to achieve acellular whole renal scaffold.

In the present study, we proposed a new rapid, effective protocol for obtaining decellularized renal scaffolds, based on consecutive perfusions of the explanted kidneys with 2 different detergents, each lasting 1.5 h and intermitted by a 1 h wash with PBS. Several methods have been developed for removing cells from whole organs[25-27] but the one developed in our study is the most rapid means for achieving complete decellularization without altering the morphological and biochemical characteristics of the ECM.

The two detergents we used have distinct chemical properties. Triton X-100, a mild non-ionic detergent capable of solubilizing proteins, was used first to produce lysis of cell

FIGURE 8. Histological findings of explanted renal ECM-based scaffold H&E staining demonstrates the presence of a strong inflammatory reaction especially in the renal pericapsular areas (**A, B, C**). Glomerula and vessel morphology are still preserved after seven days but completely fill full by clotted material (**C, D**). Magnification (**A**) 5x; (**B, C**) 10x; (**D**) 20x.

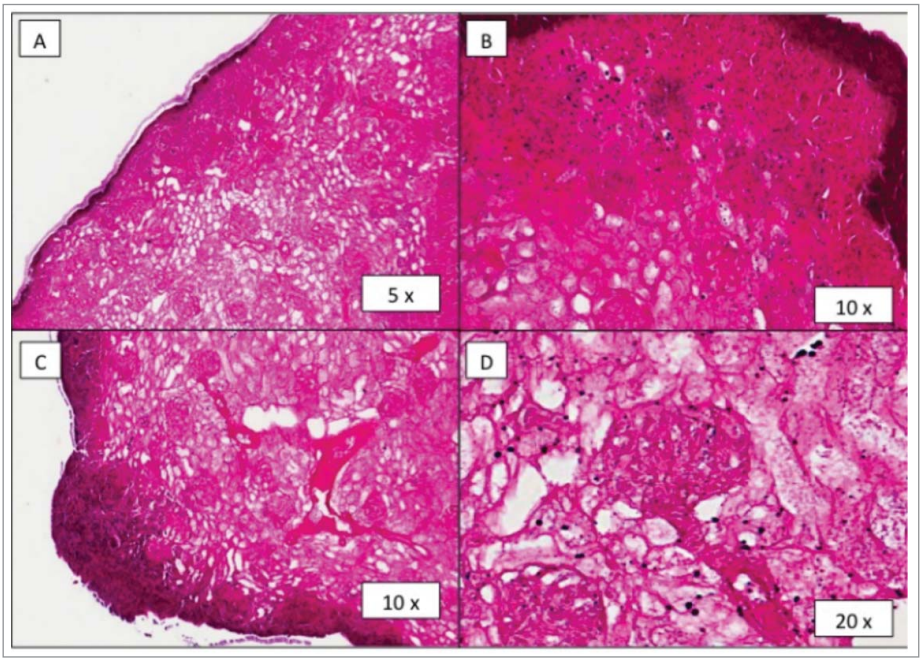

membranes with release of the cytoplasmic material. Its main advantage is that, like all nonionic detergents, it is ionically inert.[26] A recent review of the literature revealed contradictory findings on the effects of this detergent on ECM collagens: in some studies it was associated with loss of collagens and laminin, whereas in others it seems to preserve these components after cell removal.[28] The second detergent we used, SDS, is a more powerful anionic detergent that is capable of removing the entire cell component rapidly and effectively while preserving the composition of the ECM.[29,30]

Histological studies revealed that this protocol completely eliminated the cellular component of the whole organ while preserving the morphological and structural characteristics of the ECM, which consists mainly of collagens and laminin. DAPI staining of the samples we examined and DNA quantification revealed no residual DNA, and for this reason we did not wash our scaffolds with DNase.

Resin cast confirmed to be the ideal method to analyze and describe 3-dimensional glomerular microarchitecture permitting also to obtain an objective evaluation about morphometrical preservation of acellular glomerular structures. Our data showed that, even if glomerular morphology was well conserved between native and scaffold, group diameter and volumetric analysis revealed a statistically significative reduction in the treated group around −45%. We hypothesized that this reduction could be related to the glomerular endothelial cells removal by decellularization causing the whole structure shrinking but more investigations still need to be made to confirm this assumption. Moreover future examination on glomerular morphometric changes after repopulation will be useful to really understand the interplay between cellular populations and ECM structure.

Morphological and morphometrical preservation of the organ-specific unit, the glomerulus, is particular important for a deep understanding of renal cellular/ECM mechanobiology. Mechanobiology is an emerging scientific field that aims to comprehend the role of organic tissutal geometry and forces in regulating morphology and cellular driving

function. This area can be related to regenerative medicine as an instrument to study and highlight the importance of ECM organization maintenance. Renal ECM angioarchitecture is a plastic but perfectly organized network and its conservation, during and after the decellularization, is mandatory to preserve as much as possible ECM structural and instructional role (delivering biochemical and biomechanical signals that can influence cellular survival, migration, adhesion and phenotypic modulation).[31]

Orthotopic transplantation of the scaffolds was technically successful in all cases. The cuff technique confirmed to be an excellent choice for 3 main reasons. First, it was rapid and easy-to-do thereby reducing clamping time.[32] Second, it promotes linear blood flow through the vein, which decreases the risk of clot formation at the blood outflow site. Third, it allowed us to implant the renal graft in its exact native location, which has important implications in terms of site-specific blood pressure.

On the basis of our experience in this study, the tissue elasticity during the transplant and manageability of the scaffolds were no different from those of non-treated vessels. The arterial anastomosis also proved to be feasible, and no microsurgical technical-related problems were encountered. Leakage was observed when the microvascular clamps were removed in only one out of the 7 cases. The blood loss was minimal and probably due to leakage at the level of the anastomosis caused by the absence of the vessels' endothelial linings.

The recipient rats were sacrificed 7 d after surgery. During this period, none of the animals had displayed any type of adverse reaction. However, despite the intra- and postoperative administration of anticoagulants, the entire vascular network of the scaffolds was completely occluded by blood clots.

Repopulation of an acellular organ scaffold for transplant purposes involves 2 different subcompartments: the parenchyma, whose cells carry out the organ-specific functions, and the endothelium, which is necessary to ensure implantation and long-term perfusion of the new graft without clotting.[31] Re-vascularization seems to be the first step toward the generation of an entirely recellularized organ. Our seeding demonstrated homogenously cell distribution in the renal matrix and non-toxicity status of the scaffold. Absence of the vascular endothelial layer after transplantation allows direct contact between the blood and the ECM, which results in intense activation of the coagulation cascade and clot formation. In 2013, Song et al.[33] published a scientifically impeccable technical report on the transplantation of rodent kidney "organoids," which had been decellularized and subsequently recellularized with human umbilical venous endothelial cells (to regenerate the vascular endothelium) and rat neonatal kidney cells (to reconstitute the parenchymal compartment).

The results of this study therefore demonstrate that acellular renal scaffolds can be obtained rapidly from rat kidneys without damaging the structural architecture and biochemical properties of the ECM. The scaffolds proved to be very manageable during surgery and were successfully transplanted with no particular difficulties. Our study confirms previous findings that point to regenerative medicine and bioengineering as candidate milestones in the medicine of the future.

MATERIALS AND METHODS

A total of 33 male Lewis rats (weights: 250–350 gr, age: 3–4 months) were used for this study. 26/33 of the animals were used as organ donors for the creation of renal scaffolds. Left kidneys of these rats were explanted and decellularized. 19/26 scaffolds thus obtained were analyzed by cellular seeding test, DNA quantification, histological and immunofluorescent studies and scanning electron microscopy (SEM) and compared to native right contralateral kidneys harvested from the same animals. The other 7 were orthotopically transplanted into the 7 recipient rats (7/33). All procedures were conducted in accordance with Italian and European norms regarding the use of living animals in research.

Donor kidney harvest

Donor animals were anesthetized with isofluorane delivered via cone masks (3% for

induction, 2% during the operation, 1 L/min air flow, FiO2 70–75%). A midline xyphopubic laparotomy was performed, and the loops of the small and large intestines were displaced to the right to expose the left renal retroperitoneal area. The decision to use the left rather than the right kidney to create the scaffold was based on technical considerations related to rat anatomy. After that posterior lumbar arteries had been isolated, tied, and sectioned, the suprarenal, infrarenal, and subrenal segments of the aorta were gently dissected from the vena cava. The adrenal artery and vein and the gonadal vessels were isolated and sectioned between 7/0 silk ties. The renal artery and vein were completely isolated, down to the renal hilum. The ureter was freed from surrounding tissues and sectioned between ties, just distal to its origin. All perinephric fat was removed from the kidney. An aortic patch was maintained to ensure perfusion and side-to-end aorto-aortic anastomosis of the transplant. Ten UI of heparin were injected into animal vascular system. The graft was then removed, placed on a sterile Petri dish at 4°C, and subjected to the bench procedures described below.

The right kidney was then removed using a standard nephrectomy and analyzed as controls by histological and immunofluorescence studies and for SEM morphometrical analysis. The donor rat was then euthanized by lethal anesthetic drug injection.

Bench procedures on left kidneys

The cranial stump of the aorta was ligated with a silk tie, and a 24-G intravenous cannula was inserted into the distal segment and secured with 7/0 silk sutures. The kidney was then flushed with 30 ml of cold (4°C) heparinized saline (100 units / ml NaCl 0.9% saline) to eliminate residual intraluminal blood and any clots that had eventually formed.

With the aid of stereomicroscopy, a 14G plastic tube was used to create a cuff measuring 4 mm (main body: 3 mm plus a 1-mm extension to facilitate handling during the surgical procedure). A shallow, circumferential incision was made around the outer surface of the cuff to improve its adherence with the renal vein. The renal vein was inserted through the cuff and the latter advanced to the renal hilum. The protruding tip of the renal vein was then folded back and secured to the cuff with 7/0 silk ties (**Fig 5**).

Organ decellularization

The cellular component of the kidney was gently detached from the extracellular matrix skeleton by means of slow aortic anterograde pulsatile perfusion with ionic and anionic detergents (Triton X-100 1% and SDS 1%, both from Sigma-Aldrich, St. Louis, MO, USA). First, the Triton X-100 (100 mL) was infused (room temperature, flow rate: 70 ml / h) with a peristaltic pump (Minipulse 2 – Gilson, Inc., Middleton, WI, USA). All traces of the Triton X-100 were then eliminated with an intermediate perfusion with 50 ml of PBS (Sigma-Aldrich, St. Louis, MO, USA) (flow rate: 50 ml/h). The graft was then perfused with 100 ml SDS 1% (room temperature, flow rate: 70 ml/h) and subjected to a final pulsatile perfusion with 50 ml PBS (flow rate: 50 ml/h). The decellularized scaffold was placed in PBS and stored at 4°C.

Histological and Immunofluorescence assessment of the scaffolds

Histological and immunofluorescence studies were performed on 7/26 of the renal scaffolds obtained as described above and (for comparison purposes) on the native right kidneys from the same animals used to obtain the scaffolds.

Decellularized and control samples were fixed in 10% formalin, dehydrated in 60% ethanol, embedded, 5 μm sectioned and stained with hematoxylin and eosin (H&E). The DNA-binding fluorescent stain 4′,6′-diamidino-2-phenylindole (DAPI) was used to exclude the presence of cells and residual traces of DNA. Masson Trichrome (Newcomer Supply, Middleton, WI, USA), Picrosirius red (Polysciences, Inc., Warrington, PA, USA), and Alcian blue staining (Sigma-Aldrich, St. Louis, MO, USA) were used to demonstrate collagen fibrils and proteoglycans (mucins) in the ECM.

Immunofluorescence assays were carried out on decellularized and native tissues in order to evaluate the presence of specific types of collagen (types I, III, and IV), fibronectin, and laminin as previously described by Malara et al.[22] The samples were fixed in 4% paraformaldehyde (PFA) for 24 h, embedded in optimal cutting temperature (OCT) cryosectioning medium, and snap-frozen in liquid nitrogen. Eight-micron tissue sections were prepared with a Microm Microtome HM 250 (Bio Optica S.p.A., Milan, Italy). Sections used for immunofluorescence staining were fixed for 20 min in 4% PFA, washed with PBS, and blocked for 30 min with 2% bovine serum albumin (BSA) (Sigma-Aldrich, Milan, Italy) in PBS. Nonspecific binding sites were saturated by incubating sections for 1 h with 5% goat serum, 2% BSA, and 0.1% glycine in PBS. The sections were then incubated overnight (4°C) with primary antibodies in washing buffer (0.2% PBS, 0.1% Tween 20 in PBS). After three washes, the sections were incubated with appropriate fluorescently conjugated secondary antibodies in washing buffer for 1 hour at room temperature (RT). The nuclei were counterstained with Hoechst 33258 (100 ng/mL in PBS) at RT for 3 minutes, and the sections were mounted on glass micro coverslips using Fluoro-mount (Bio Optica, Milan, Italy). Negative controls (tissues treated as described above with omission of the incubation with primary antibody) were routinely included. All images were acquired with an Olympus BX51 fluorescence microscope (Olympus Deutschland GmbH, Hamburg, Germany) and 20X/0.50 Olympus UplanF1 objectives.

Laminin evaluation was performed on 3 different groups: native (N = 2), just perfused with Triton X-100 (N = 2) and final acellular kidneys (N = 2). For each of them formalin-fixed, paraffin-embedded kidney sections were cut (5 μm thick). The slides were deparaffinized and subjected to heat induced antigen retrieval microwaving for 10 minutes. Laminin was assessed by incubating kidney slides sections with the specific primary antibody (1:25, Sigma-Aldrich) for 1 hour at 37°C. Samples were then co-stained with Hoechst (Life Technologies).

All the stained slides were evaluated with a fluorescent microscope (Zeiss Observer zv1, Zeiss, Germany) and digital images were acquired with 20X magnification using dedicated software (Axiovision Zeiss, Germany; http://www.zeiss.com/microscopy/en_de/downloads/axiovision.html).

Residual collagenic status of the scaffolds was evaluated using Sircol Soluble Collagen Assay Kit (Biocolor Ltd., Carrickfergus, UK). After a 12 h solubilization in acid-pepsin enzymatic solution, collagens were conjugated with Sircol Kit reagents and then measured by an absorbance of 555 nm using Spectramax M5 Multi-Mode Microplate Reader (Molecular Device Inc., Sunnyvale, CA).

DNA quantification

In order to evaluate the quality of the decellularization process, DNA quantification was performed on 5 mg of dry samples of acellular scaffold with using Qiagen AllPrep DNA/RNA Mini Kit (cat. No. 80204; Qiagen Inc., Valencia, CA). Control values were obtained from 5 mg of native kidneys by the same protocol. DNA achieved from both groups was quantified with Nano Drop technology. DNA quantification was performed on a total of 6 samples (3 native kidneys and 3 acellular scaffolds).

Morphometrical analysis of corrosion-casted glomerular samples

Corrosion precasting treatment was completed on 3 native kidneys and on 3 scaffolds by gradually flushing each of them with 10 ml of heparinized 0.9% NaCl solution to completely remove blood (or detergents for the scaffolds) from the vascular tree. They were then manually injected with 4–7 ml of specific casting resin obtained by adding to the main solution (Batson's #17 Monomer Base Solution, Cat. No. #02599, PoliScience Inc., Warrington, PA, USA) dedicated promoter and catalyst solution (Batson's #17 Anatomical Corrosion Kit Promoter Cat. No. #02608; Batson's #17 Anatomical Corrosion kit Catalyst, Cat. No. #02610

PolyScience Inc., Warrington, PA, USA) until satisfying venous reflux was detected. Polymerization started and kidneys were placed in room temperature deionized water overnight. Subsequently all the surrounding perivascular tissue was chemically detached by 2 rinses (24 h each) of concentrated sodium hydroxide solution (10% and 5% respectively). After that casted samples were air-dried, in a Petri dish, for 24 h at room temperature. All the specimens were coated with gold and Scanning Electron Microscopy (SEM) was used to explore 10 randomly selected areas for each sample. Glomerular images were acquired for a total of 30 glomerula for the Group 1 (Native) and 30 glomerula for the Group 2 (Decellularized) and all the images were managed and studied with Image J Software (http://imagej.nih.gov/ij/). Glomerular afferent and efferent arteriolar diameters were measured for three different points in each glomerulus and averaged. Glomerular images were then bounded. Using an averaged ray and handling each of them as a sphere, resultant volumes were finally estimated and used for statistical analysis comparing Group 1 and Group 2.

Dynamic recellularization of renal scaffold and renal scaffold cytotoxicity

Human pancreatic carcinoma cells (MIA PaCa-2) (4 million) were dynamically seeded in a custom-made bioreactor to test eventual extracellular matrix cytotoxicity. After decellularization renal scaffold was flushed with PBS overnight to fully remove residual detergent cells were then manually injected through renal arterial vascular network and kidney was inserted in a custom-made bioreactor at constant temperature of 37°C. The organ was perfused with specific medium for 24 h with flow rate of 1 ml/min. Specimens were then formalin-fixed and histologically analyzed by H&E and DAPI staining.

Scaffold implantation in recipient rats

The 7/21 remaining renal scaffolds were orthotopically transplanted into the Group 2 animals. The procedures were performed with isofluorane anesthesia (Fluovac; Veterinarian Fluosorber; The Harvard Apparatus) after induction with an intramuscular injection of zolazepam/tiletamine, 6.6 mg/kg of each (Zoletil, Virbac Corp., Fort Worth, TX). The skin was disinfected with povidone iodine, and a midline laparotomy was performed. The loops of the small and large intestines were displaced to the right to expose the left renal retroperitoneal area. The recipient's renal vein was dissected to the hilum, and the suprarenal, renal, and subrenal segments of the aorta were mobilized. A vascular microclamp was placed on either side of the proximal and distal aorta, and a third clamp was positioned on the inferior vena cava (IVC) side of the renal vein. The vein was then cut at the hilum to preserve as much venous tissue as possible, thereby facilitating rapid cuff-technique venous anastomosis. The renal artery and the ureter were sectioned between 7/0 silk ties, and the left kidney removed.

The renal scaffold was then positioned in the left renal fossa of the recipient, and 2 units/kg of heparin were administered through penile vein. The venous anastomosis was created by inserting the cuff into the recipient renal vein and securing it with a 7–0 silk suture. An aorto-aortic end-to-side anastomosis was then performed with a 9–0 Prolene running sutures. The microclamps were removed (venous first, then arterial), and the scaffold was completely reperfused. The anastomosis site was carefully inspected and additional sutures added to correct any bleeding that was observed. The large and small intestines were replaced and the abdomen closed in anatomical layers.

The animals were kept on heating pads (37.5°C) for the first 1.5–2 hours after surgery and then transferred to their cages until they had recovered completely from the anesthesia. After a 12-h fast, they were allowed free access to food and water. For 7 d after the procedure heparin was subcutaneously administered to the animal (2 units/kg) daily. On postoperative day 7, the animals were sacrificed by a lethal anesthetic drug injection and the grafts removed for histological analysis.

Statistics

Continuous data were presented as mean values ± STD. For all the analysis (DNA laminin and collagen quantification and glomerular morphometric studies), for non-parametric values Mann Whitney T-Test was used.

DISCLOSURE OF POTENTIAL CONFLICTS OF INTEREST

No potential conflicts of interest were disclosed.

AUTHOR CONTRIBUTIONS

Andrea Peloso designed and wrote the project, performed surgeries; collected results, interpreted data and wrote the manuscript. Jacopo Ferrario designated and wrote the part of the project concerning surgical procedures, performed surgeries and edited the relative paragraph of the manuscript. Benedetta Maiga, Ilaria Benzoni and Carolina Bianco performed surgeries, completed decellularization process and revised the manuscript critically. Antonio Citro and Lorenzo Piemonti provided inputs on scaffold biology, performed extracellular matrix histological characterization wrote the relative part of the manuscript and revised it critically. Manuela Currao, Alessandro Malara and Alessandra Balduini performed extracellular matrix immunofluorescent characterization, wrote the relative part of the manuscript and revised it critically. Annalisa Gaspari took care of the animal's health after the surgical procedure. Massimo Abelli, Giuseppe Orlando, Paolo Dionigi and Marcello Maestri co-designed the project, provided inputs about surgical procedures, edited the manuscript and revised it critically.

References

1. Willet JD, Pichitsri W, Jenkinson SE, Brain JG, Wood K, Alhasan AA, Spielhofer J, Robertson H, Ali S, Kirby JA. Kidney transplantation: analysis of the expression and T cell mediated activation of latent TGF-β. J Leukoc Biol 2013; 93:471-8; PMID:23192429; http://dx.doi.org/10.1189/jlb.0712324
2. Ingelfinger JR, Alexander SI. One step closer to "Rejectostix". N Engl J Med. 2013; 369:84-5; PMID:23822781; http://dx.doi.org/10.1056/NEJMe1307013
3. Grzelak P, Szymczyk K, Strzelczyk J, Kurnatowska I, Sapieha M, Nowicki M, Stefanczyk L. Perfusion of kidney graft pyramids and cortex in contrast-enhanced ultrasonography in the determination of the cause of delayed graft function. Ann Transplant 2011; 16:48-53; PMID:21436774
4. Dantal J, Soulillou JP. Immunosuppressive drugs and the risk of cancer after organ transplantation. N Eng J Med 2005; 352:1371-3; http://dx.doi.org/10.1056/NEJMe058018
5. United States Renal Data System. Excerpts from USRDS 2009 annual data report. U.S. Department of Health and Human Services. The National Institutes of Health, National Institute of Diabetes and Digestive and Kidney Diseases. Am J Kidney Dis 2010; 55 (suppl 1).
6. Serur D, Charlton M. Expanded criteria living donors: how far can we go? Prog Transplant 2012; 22:129-32; PMID:22878068; http://dx.doi.org/10.7182/pit2012244
7. Molnar MZ, Streja E, Kovesdy CP, Shah A, Huang E, Bunnapradist S, Krishnan M, Kopple JD, Kalantar-Zadeh K. Age and the associations of living donor and expanded criteria donor kidneys with kidney transplant outcomes. Am J Kidney Dis 2012; 59:841-8; PMID:22305759; http://dx.doi.org/10.1053/j.ajkd.2011.12.014
8. Reich DJ, Guy SR. Donation after cardiac death in abdominal organ transplantation. Mt Sinai J Med 2012; 79:365-75; PMID:22678860; http://dx.doi.org/10.1002/msj.21309
9. Deng R, Gu G, Wang D, Tai Q, Wu L, Ju W, Zhu X, Guo Z, He X. Machine perfusion versus cold storage of kidneys derived from donation after cardiac death: a meta-analysis. PLoS One 2013; 8(3): e56368.
10. Daar AS, Greenwood HL. A proposed definition of regenerative medicine. J Tissue Eng Regen Med 2007; 1:179-84; PMID:18038409; http://dx.doi.org/10.1002/term.20
11. Atala A. Engineering organs. Curr Opin Biotechnol 2009; 20:575-92; PMID:19896823; http://dx.doi.org/10.1016/j.copbio.2009.10.003
12. Vacanti JP, Langer R. Tissue engineering: the design and fabrication of living replacement devices for surgical reconstruction and transplantation. The Lancet 1999; 354:32-34; http://dx.doi.org/10.1016/S0140-6736(99)90247-7

13. MacNeill BD, Pomerantseva I, Lowe HC, Vacanti JP. Toward a new blood vessel. Vasc Med 2002; 7(3): 241-6; PMID:12553747; http://dx.doi.org/10.1191/1358863x02vm433ra
14. Jungebluth P, Moll G, Baiguera S, Macchiarini P. Tissue-engineered airway: a regenerative solution. Clin Pharmacol Ther 2012; 91:81-93; PMID:22130120; http://dx.doi.org/10.1038/clpt.2011.270
15. Atala A, Bauer SB, Soker S, Yoo JJ, Retik AB. Tissue-engineered autologous bladders for patients needing cystoplasty. Lancet 2006; 367:1241-6; PMID:16631879; http://dx.doi.org/10.1016/S0140-6736(06)68438-9
16. Badylak SF, Taylor D, Uygun K. Whole-organ decellularization and recellularization of three-dimensional matrix scaffolds. Annu Rev Biomed Eng 2011; 13:27-53; PMID:21417722; http://dx.doi.org/10.1146/annurev-bioeng-071910-124743
17. Booth C, Soker T, Baptista P, Ross CL, Soker S, Farooq U, Stratta RJ, Orlando G. Liver bioengineering: current status and future perspectives. World J Gastroenterol 2012; 18:6926-34; PMID:23322990; http://dx.doi.org/10.3748/wjg.v18.i47.6926
18. Chen H, Liu Y, Jiang Z, Chen W, Yu Y, Hu Q. Cell-scaffold interaction within engineered tissue. Exp Cell Res 2014, 323:346-51; PMID:24631290; http://dx.doi.org/10.1016/j.yexcr.2014.02.028
19. Ott HC, Matthiesen TS, Goh SK, Black LD, Kren SM, Netoff TI, Taylor D. Perfusion-decellularized matrix: using nature platform to engineer a bio-artificial heart. Nat Med 2008; 14:213-21; PMID:18193059; http://dx.doi.org/10.1038/nm1684
20. Ren H, Shi X, Tao L, Xiao J, Zhang Y, Yuan X, Ding Y. Evaluation of two decellularization methods in the development of a whole-organ decellularized rat liver scaffold. Liver int 2013; 33:448-58; PMID:23301992; http://dx.doi.org/10.1111/liv.12088
21. Maghsaudlou P, Totinelli G, Lankogeargakis SP, Eaton S, De Coppi P. A decellularization methodology for the production of a natural acellular intestinal matrix. J Vis Exp 2013; 7:80
22. Malara A, Currao M, Gruppi C, Celesti V, Viarengo G, Buracchi C, Laghi L, Kaplan DL, Balduini A. Megakaryocytes contribute to the bone marrow-matrix environment by expressing fibronectine, type IV collagen and laminin. Stem Cells 2014; 32:926-37; PMID:24357118; http://dx.doi.org/10.1002/stem.1626
23. Badylak SF, Gilbert TW. Immune response to biologic scaffold materials. Seminars in Immunology. Amsterdam Elsevier 2008; 109-116
24. Ishii E, Shimizu A, Takahashi M, Terasaki M, Kunugi S, Nagasaka S, Terasaki Y, Ohashi R, Masuda Y, Fukuda Y. Surgical technique of orthotopic liver transplantation in rats: the Kamada technique and a new splint technique for hepatic artery reconstruction. J Nippon Med Sch 2013; 80:4-15.
25. Caralt M, Uzarski JS, Iacob S, Obergfell KP, Berg N, Bijonowski BM, Kiefer KM, Ward HH, Wandinger-Ness A, Miller WM, et al. Optimization and critical evaluation of decellularization strategies to develop renal extracellular matrix scaffolds as biological templates for organ engineering and transplantation. Am J Transplantation 2015; 15:64-75; http://dx.doi.org/10.1111/ajt.12999
26. Jiang WC, Cheng YH, Yen MH, Chang Y, Yang VW, Lee OK. Cryo-chemical decellularization of the whole liver for mesenchymal stem cells-based functional hepatic tissue engineering. Biomaterials 2014; 35:3607-17; PMID:24462361; http://dx.doi.org/10.1016/j.biomaterials.2014.01.024
27. Bonandrini B, Figliuzzi M, Papadimou E, Morigi M, Perico N, Casiraghi F, Dipl C, Sangalli F, Conti S, Benigni A, et al. Recellularization of well-preserved acellular kidney scaffold using embryonic stem cells. Tissue Eng Part A 2014; 20:1486-98; PMID:24320825; http://dx.doi.org/10.1089/ten.tea.2013.0269
28. Gilbert TW, Sellaro TL, Badylak SF. Decellularization of tissue and organs. Biomaterials 2006; 27:3675-83; PMID:16519932
29. Cartmell JS, Dunn MG. Effect of chemical tretaments on tendon cellularity and mechanical properties. J Biomed Mater Res 2000; 49:134-40; PMID:10559756; http://dx.doi.org/10.1002/(SICI)1097-4636(200001)49:1%3c134::AID-JBM17%3e3.0.CO;2-D
30. Gratzer PF, Harrison RD, Woods T. Matrix alterations and not residual sodium dodecyl sulfate cytotoxicity affects the cellular repopulation of a decellularized matrix. Tissue Eng 2006; 12:2975-83; PMID:17518665; http://dx.doi.org/10.1089/ten.2006.12.2975
31. Humphrey JD, Dufresne ER and Schwartz MA. Mechanotransduction and extracellular matrix homeostasis. Nat Rev Mol Cell Biol 2014; 15:802-812; PMID:25355505; http://dx.doi.org/10.1038/nrm3896
32. Chen H, Zhang Y, Zheng D, Praseedon RK, Dang J. Orthotopic kidney transplantation in mice: technique using cuff for renal vein anastomosis. Plos One 2013; 14:8
33. Song JJ, Guyette JP, Gilpin SE, Gonzalez G, Vacanti JP, Ott HC. Regeneration and experimental orthotopic transplantation of a bioengineered kidney. Nat Med 2013; 19:646-51; PMID:23584091; http://dx.doi.org/10.1038/nm.3154